

# The search for high-mass X-ray binaries in the Phoenix dwarf galaxy

E. S. Bartlett,<sup>1\*</sup> M. J. Coe,<sup>1</sup> F. Haberl,<sup>2</sup> V. A. McBride<sup>1</sup> and R. H. D. Corbet<sup>3</sup>

<sup>1</sup>*School of Physics and Astronomy, University of Southampton, Highfield, Southampton SO17 1BJ*

<sup>2</sup>*Max-Planck-Institut für Extraterrestrische Physik, Giessenbachstraße 85748, Germany*

<sup>3</sup>*X-ray Astrophysics Laboratory, University of Maryland Baltimore County, Mail Code 662, NASA Goddard Space Flight Center, Greenbelt, MD 20771, USA*

Accepted 2012 February 20. Received 2012 February 4; in original form 2011 March 4

## ABSTRACT

We report on the first X-ray images of the Phoenix dwarf galaxy, taken with *XMM–Newton* in 2009 July. This Local Group dwarf galaxy shares similarities with the Small Magellanic Cloud (SMC) including a burst of star formation  $\sim 50$  Myr ago. The SMC has an abundance of high-mass X-ray binaries (HMXBs) and so we have investigated the possibility of an HMXB population in Phoenix with the intention of furthering the understanding of the HMXB–star formation rate relation. The data from the combined European Photon Imaging Cameras (EPIC) were used to distinguish between different source classes [foreground stars, background galaxies, active galactic nuclei (AGN) and supernova remnants] using EPIC hardness ratios and correlations with optical and radio catalogues. Of the 81 X-ray sources in the field of view, six are foreground stars, four are galaxies and one is an AGN. The remaining sources with optical counterparts have  $\log(f_X/f_{\text{opt}})$  consistent with AGN in the local Universe. Further investigation of five sources in the field of view suggests that they are all background AGN. Their position behind the gas cloud associated with Phoenix makes them a possible tool for further probing the metallicity of this region. We find no evidence for any HMXBs in Phoenix at this time. This rules out the existence of the X-ray persistent supergiant X-ray binary systems. However, the transient nature of the Be/X-ray binaries means we cannot rule out a population of these sources but can conclude that it is not extensive.

**Key words:** galaxies: individual: Phoenix dwarf – X-rays: binaries – X-rays: galaxies.

## 1 INTRODUCTION

The Phoenix dwarf galaxy was discovered in 1976 by Schuster & West who described it as a very distant ( $\sim 100$  kpc) globular cluster. It was later identified as a dwarf irregular galaxy (dIrr) by Canterna & Flower (1977). These galaxies are H I rich and show obvious signs of recent star formation. Despite this classification, Phoenix has characteristics of a dwarf spheroidal galaxy (dSph) and it has been suggested that it belongs to an intermediate class of galaxy between the dwarf spheroidal and dwarf irregular, along with three other dwarf galaxies [Pegasus, Pisces (LGS3) and Antila]. The distance to Phoenix has been determined to be  $\sim 420$  kpc using a variety of different methods and data sets (for example, see van de Rydt, Demers & Kunkel 1991; Martínez-Delgado, Gallart & Aparicio 1999 and, more recently, Menzies et al. 2008), placing Phoenix well within the Local Group.

The H I gas surrounding Phoenix was mapped by Young & Lo (1997) and Young et al. (2007) using the Very Large Array (VLA). They identify several regions in the immediate vicinity with a va-

riety of shapes and velocities. One such cloud, located  $\sim 5$  arcmin south-west of the main stellar body, has been unequivocally associated with Phoenix based on the excellent agreement of the radial velocities of the stars, obtained from stellar spectra (Irwin & Tolstoy 2002) from the Very Large Telescope (VLT), and the velocity of the H I cloud. Young et al. (2007) recognize that this offset suggests that Phoenix could offer a unique opportunity to study the possible mechanisms responsible for gas removal in dwarf galaxies, transforming a gas-rich dIrr into a gas-poor dSph.

Extensive optical data of the central region of Phoenix also exist: the Wide Field Planetary Camera (WFPC2) on-board *Hubble Space Telescope* (*HST*) has imaged the central field of the galaxy with both *F814W* and *F555W* filters (for example, see Holtzman, Smith & Grillmair 2000; Hidalgo et al. 2009, hereafter H09). Young et al. (2007) use both of these data sets to derive separate star formation histories for the eastern and western sides of Phoenix. They report an asymmetry in the star formation rate (SFR) across the face of the galaxy, in agreement with Martínez-Delgado et al. (1999). The western side of Phoenix displays evidence for strong episodes of star formation at 180 and 40 Myr ago, whilst the eastern side shows evidence for more continual star formation from 250 to 50 Myr ago. They note that this is consistent with the H I location, offset

\*E-mail: e.s.bartlett@soton.ac.uk

to the west of the galaxy's optical emission. These epochs of star formation are similar to those for another dIrr galaxy: the Small Magellanic Cloud (SMC). Harris & Zaritsky (2004) report that the SMC had 'bursts' of star formation at 2.5, 0.4 and 0.06 Gyr in the past. In fact, the Phoenix dwarf galaxy shares many other common features with the SMC, including its low metallicity ( $Z = 0.004$  for the SMC; Russell & Dopita 1992;  $Z = 0.0015$  for Phoenix: H09).

The SMC is  $\sim 100$  times as massive as Phoenix and host to an unusually high number of high-mass X-ray binaries (HMXBs; Coe et al. 2005). These are stellar systems in which a compact object, usually a neutron star, accretes material from a more massive donor – either a supergiant or early-type star, both of OB class. Supergiant systems are a persistent source of X-rays with luminosities,  $L_X$ ,  $10^{36}$ – $10^{38}$  erg s $^{-1}$ . Be/X-ray binary systems have two types of outbursts associated with their X-ray emission. Type I outbursts have  $L_X$  in the range  $10^{36}$ – $10^{37}$  erg s $^{-1}$  and occur periodically, around the time of the periastron passage of the neutron star; Type II outbursts reach higher luminosities,  $L_X \geq 10^{37}$  erg s $^{-1}$ , and show no correlation with orbital phase (Stella, White & Rosner 1986). A comparison with the Milky Way suggests we see a factor of  $\sim 50$  more HMXBs in the SMC than we would expect to observe, based on the mass ratio of the two galaxies.

The stellar winds of massive stars are known to be line driven (Lucy & Solomon 1970) and so a lower metallicity will lead to less mass being lost from the compact object progenitor. This in turn is expected to affect the number of systems that survive the initial supernova explosion and go on to form HMXBs. Dray (2006) uses simulations to demonstrate that this is indeed the case but is unable to replicate the number and period distribution of the SMC HMXBs with a low-metallicity environment alone. It has been known for some time that HMXBs are strong tracers of recent star formation episodes in a galaxy. It is currently thought that an increase in star formation, possibly caused by tidal interactions with the Milky Way and/or the Large Magellanic Cloud (LMC) (Harris & Zaritsky 2004), along with the low metallicity of the SMC has given rise to the large number of HMXBs in the SMC. Grimm, Gilfanov & Sunyaev (2003, hereafter G03) have quantified this relationship for sources with X-ray luminosities in excess of  $10^{38}$  erg s $^{-1}$ . However Be/X-ray binaries, which are the most numerous subclass of HMXBs (Liu, van Paradijs & van den Heuvel 2006), do not reach these luminosities. One of the reasons for choosing such a high threshold luminosity was to avoid contamination from any low-mass X-ray binaries (LMXBs) present in any of the galaxies studied. Gilfanov (2004) has shown that the number of LMXBs scales linearly with the mass of the host galaxy; therefore, the low-mass Local Group dwarf galaxies like Phoenix ( $3.3 \times 10^7 M_\odot$ ; Mateo 1998), which are too low mass to expect LMXBs, are ideal for probing the HMXB–star formation relation in the low luminosity limit. By studying any population present we hope to further understand factors that can influence star formation in such diverse environments.

Predicting the number of HMXBs cannot be done with great accuracy as the effects of all the influencing parameters are not fully understood. If we assume that the  $\text{Log}N$ – $\text{Log}S$  relationship reported by G03 for HMXBs remains valid down to X-ray luminosities of  $5 \times 10^{35}$  erg s $^{-1}$ , the typical luminosity of the lower type I outbursts seen in the SMC (Haberl et al. 2008a), equation (7) of G03 and the average SFR of Phoenix ( $1 \times 10^{-3} M_\odot \text{yr}^{-1}$ , calculated from data in H09) predicts  $0.14 \pm 0.02$ . However, this apparently precise number could be significantly affected by many factors including the metallicity values. The same equation predicts  $\sim 20$  X-ray sources with  $L_X > 5 \times 10^{35}$  erg s $^{-1}$  (adopting the same value for the SFR as G03,  $0.15 M_\odot \text{yr}^{-1}$ , taken from Yokogawa et al. 2000) for the

SMC. We currently know of  $\sim 60$  HMXBs in the SMC (Liu, van Paradijs & van den Heuvel 2005), of which  $\sim 50$  are X-ray pulsars, and more are being discovered every year (e.g. SXP1062; Hénault-Brunet et al. 2011). Using an SFR of  $0.2 M_\odot \text{yr}^{-1}$  for the LMC (Harris & Zaritsky 2009) leads to a prediction of  $\sim 30$  sources in the LMC with this luminosity constraint. There are currently 36 known HMXBs in the LMC, including several supergiant systems and black hole candidates.

The reason behind the apparent discrepancy in the SMC could lie with both the activity cycles of these HMXBs and the details of their star formation histories. The number of HMXBs in a galaxy will be more strongly linked to the recent star formation episodes, rather than the average star formation of the galaxy over its lifetime. The SFR of the more recent episodes of star formation (40–60 Myr ago) in Phoenix and the SMC is very similar. The SMC varies from  $8.1 \pm 1.4 \times 10^{-5}$  to  $1.5 \pm 0.6 \times 10^{-5} M_\odot \text{yr}^{-1} \text{arcmin}^{-2}$  (Antonioni et al. 2010) depending on the area of the SMC, whilst the most recent epoch of star formation in Phoenix had an SFR of  $2.5 \pm 1.8 \times 10^{-5} M_\odot \text{yr}^{-1} \text{arcmin}^{-2}$  (Young et al. 2007). It is only by probing galaxies across a broad spectrum of mass, star formation history and chemical composition that we can establish both trends in the HMXB populations of these galaxies and understand the significance of these objects as tracers of star formation.

## 2 OBSERVATIONS AND DATA REDUCTION

The first X-ray images of the Phoenix dwarf galaxy were taken with *XMM-Newton* during the satellite revolution 1754 on 2009 July 7. This paper will discuss the data collected with the European Photon Imaging Camera (EPIC) MOS (Turner et al. 2001) and pn (Strüder et al. 2001) detectors. All detectors were operating in full window modes, giving a field of view of  $\sim 30$ -arcmin diameter. Table 1 summarizes the details of the EPIC observations. The data were processed using the *XMM-Newton* Science Analysis System v9.0 along with software packages from FTOOLS v6.8.

The MOS and pn observational data files were processed with EMPROC and EPPROC, respectively. Periods of high background activity were screened by removing any times when the count rate above 10 keV was  $>0.8$  count s $^{-1}$  for the MOS detectors and  $>2.0$  count s $^{-1}$  for the pn detector. The filtered event files were then split into five energy bands – (0.2–0.5), (0.5–1.0), (1.0–2.0), (2.0–4.5) and (4.5–12.0) keV – to identify and discriminate between hard and soft sources in the field of view. For the pn detector, we selected only the 'single' (PATTERN = 0) pixel event patterns in the range 0.2–0.5 keV, for all the other bands 'single and double' (PATTERN  $\leq 4$ ) pixel events were accepted. For the MOS, 'single' to 'quadruple' (PATTERN  $\leq 12$ ) pixel events were selected.

For all detectors we created images, background and exposure maps in each of the five energy bands. A box sliding detection was performed simultaneously on all 15 images (five energy bands for each of the MOS1, MOS2 and pn cameras) with the task EBOXDETECT as a precursor to the maximum likelihood fitting task EMLDETECT. The maximum likelihood fitting yielded 90 sources in the field of

**Table 1.** *XMM-Newton* EPIC observations of the Phoenix galaxy on 2009 July 7.

Camera	Filter	Read-out mode	Observation		Exp. (ks)
			Start	End (UT)	
MOS1/2	Medium	FF, 2.6 s	08:13	21:11	46.6
pn	Thin1	FF, 73 ms	08:36	21:06	45.0

view, each with a total detection likelihood larger than 10. This corresponds to a probability of a source being a spurious detection of  $\sim 5 \times 10^{-5}$  in a single image, and  $3 \times 10^{-6}$  for the case of simultaneously using 15 images.<sup>1</sup> The data were screened by eye to remove obvious false detections caused by instrumental effects, resulting in a final list of 81 sources.

To convert source count rates into flux values, the energy conversion factors (ECFs) from the *XMM-Newton* Serendipitous Source catalogue (Watson et al. 2009) were used. Whilst these ECFs do assume a spectrum typical for an AGN with low absorption, Pietsch et al. (2004, hereafter P04) show that the ECFs calculated for a typical supernova remnant (SNR; an absorbed 1-keV thin thermal spectrum) and supersoft source (SSS; absorbed 30-eV blackbody spectrum) in M33 only vary from those calculated for a typical hard source by about 20 per cent for both EPIC detectors. The flux values calculated using the ECFs are used in source classification (see Section 3) over a broad energy range (0.2–4.5 keV, bands 1–4) to be consistent with the findings of Maccararo et al. (1988) and the method of P04. A large deviation from a power-law spectrum would be required for these results to be inadequate over such a range. The flux values for band 5 are calculated, but are not used in the source classification.

Four of the X-ray-brightest sources (for exact details on which sources, see Section 5) were identified with  $>500$  counts in the full energy range (0.2–12.0 keV) across all three detectors and were subject to further spectral analysis. EPIC spectra were extracted for the pn (PATTERN  $\leq 4$ ) and both MOS (PATTERN  $\leq 12$ ) detectors, bad pixels and columns were disregarded (FLAG = 0) and intervals of high background were removed. All four sources were close to the centre of the field of view and as such were extracted with circular source regions with radius 20 arcsec.

For the MOS detectors, the background spectra were taken from an annulus surrounding the source extraction region with an outer radius of 60 arcsec. Where this was not possible, due to the proximity of other sources in the field, regions on the same chip which contained no sources were identified. Light curves and spectra were extracted (with radius 60 arcsec) from these regions and examined to confirm that they were statistically identical. The spectrum from the closest region to a source was used as the background spectrum. For the pn detector, regions on neighbouring chips which contained no sources were identified and again were confirmed to be statistically identical. As with the MOS detectors, the spectrum from the closest region to a source was used as the background spectrum. The area of source and background regions was calculated using the BACKSCAL task. Response matrix files were created for each source using the tasks RMFGEN and ARFGEN.

### 3 SOURCE CLASSIFICATION

The positions of the 81 X-ray sources in Phoenix were cross-correlated with the Local Group Galaxy Survey (LGGS; Massey et al. 2007) catalogue and the separation to the nearest optical match calculated. This was compared with the number of matches found with a simulated catalogue. The simulated positions were generated by independently reassigning both the right ascensions and declinations of all the optical sources. Fig. 1 shows the results of the correlations as a function of search radius. The solid line shows the difference between the number of X-ray sources matched with

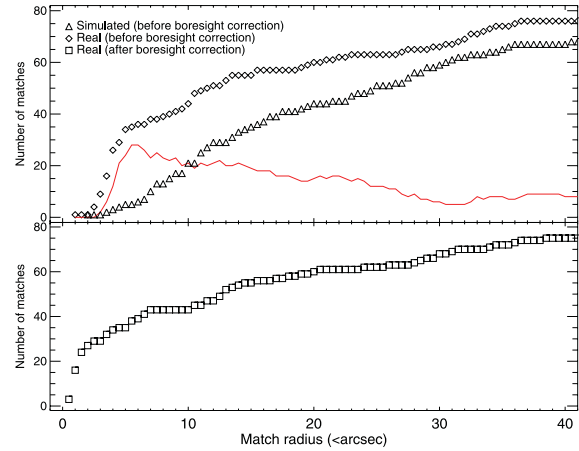


**Figure 1.** The top panel shows the cumulative number of matches as a function of search radius between the LGGS catalogue and the positions of the X-ray sources (diamonds). The number of matches between the X-ray positions and the simulated optical catalogue are also plotted (triangles). The solid red line is the difference between these two values. The bottom panel shows the number of matches between the LGGS catalogue and the boresight-corrected X-ray positions are shown for comparison (squares).

the real catalogue and the number matched with the simulated catalogue. The radius at which the number of real matches increases at the same rate as the number of simulated matches, i.e. the radius at which the solid line plateaus, can be considered as the maximum search radius. At radii greater than this value, all matches with the real catalogue are false associations. Our figure indicates that this occurs at about 6 arcsec.

The source classification described in this section was performed in two stages. The SIMBAD and NASA/IPAC Extragalactic Database (NED) archives and the LGGS and United States Naval Observatory B1.0 (USNO B1.0; Monet et al. 2003) catalogues were searched for correlations around the X-ray source positions. The preliminary classification used a search radius of up to 6 arcsec for all sources. This was primarily to identify galaxies and AGN for an astrometric boresight correction. Foreground stars were purposely not used when performing the boresight correction due to the possibility of proper motion. The four galaxies and possible AGN listed in Section 4.2 identified from the SIMBAD and NED data bases were used along with the SAS task EPOSCORR to obtain accurate positions for all our sources. The final boresight correction was  $4''.7 \pm 1''.5$ . The bottom panel of Fig. 1 shows the number of matches between the corrected X-ray positions and the LGGS catalogue for comparison. The gradient of the curve decreases dramatically after 2 arcsec, indicating that our boresight correction has been successful and that the error on our X-ray source positions is dominated by the required coordinate shift. This error is added quadratically to the statistical error derived in the source detection. The classification was then performed for a second time, using the individual  $3\sigma$  error circles as the search radius for each source. Fig. 2 shows the combined EPIC image in the 0.2–4.5 keV energy range with H I contours from Young et al. (2007) superimposed. Also shown in this figure is the combined RVB band optical image from the LGGS. The positions of the sources detected by the analysis are also displayed (the boresight-corrected positions on the optical image and the uncorrected positions on the X-ray image) along with a unique identification number for each source.

In order to locate any candidate HMXBs in Phoenix, it is necessary to identify as many of the foreground stars and background

<sup>1</sup> <http://xmm.esa.int/sas/current/doc/emldetect/index.html>

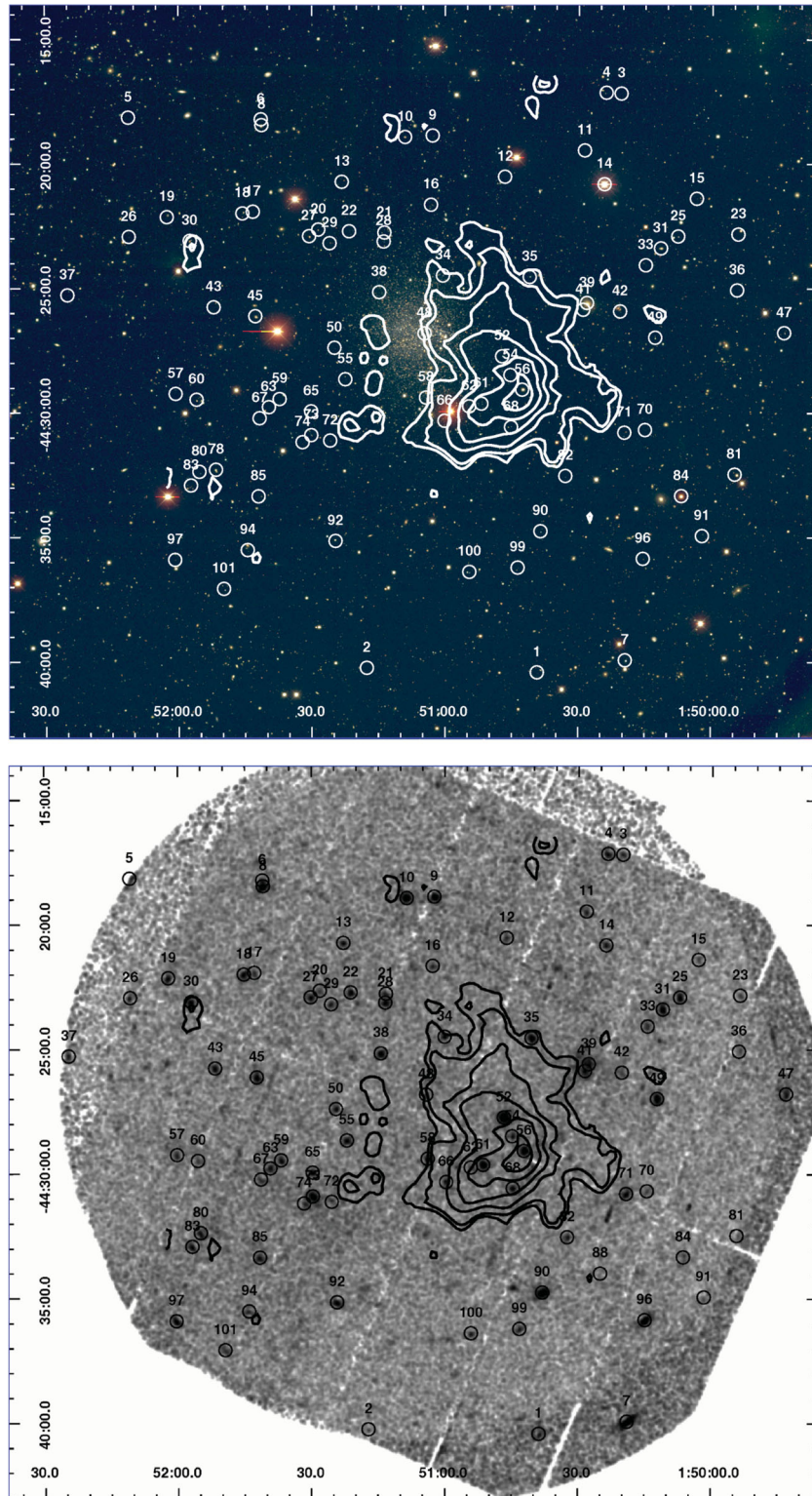


**Figure 2.** The top panel shows the optical LGGs image, the bottom panel shows the combined 0.2–4.5 keV EPIC data. H I contours from Young et al. (2007) are overlaid on both images. The contour levels correspond to column densities  $(0.5, 1, 2, 3, 4, 5) \times 10^{19} \text{ cm}^{-2}$ . The circles are the positions of the sources detected by the box sliding and maximum likelihood detection analysis, they are not indicative of the size of the error circles and are illustrative only.

sources in our field of view as possible. Following the method of P04, we attempt to identify or classify all the X-ray sources in the field of view as either foreground stars (fg stars), AGN, galaxies (GAL), SSS, SNRs or hard sources (which could be HMXBs or unidentified AGN).

P04 use the hardness ratios (HRs) of the sources (both known and unknown) in M33 to create X-ray colour plots and identify areas of specific source class. The limitations of this method of source classification are discussed in detail in P04, the main drawback being that sources with similar spectra (e.g. foreground stars and SNRs,

HMXBs and AGN) cannot be differentiated when the statistics are low. An alternative to HR classification is the quantile analysis technique of Hong, Schlegel & Grindlay (2004); however, this is not suitable for *XMM-Newton* data due to the high background. The HRs are defined as  $HR_i = (B_{i+1} - B_i)/(B_{i+1} + B_i)$ , where  $B_i$  is the count rate in energy band  $i$ . The bands are the same as those used in the source detection: (0.2–0.5), (0.5–1.0), (1.0–2.0), (2.0–4.5) and (4.5–12.0) keV. To improve the statistics, the counts from all three EPIC instruments were combined before HRs are calculated. The hydrogen column density in the direction of M33 is a factor of 4 greater than that towards Phoenix ( $1.5 \times 10^{21} \text{ cm}^{-2}$  for Phoenix and  $6 \times 10^{21} \text{ cm}^{-2}$  for M33; Dickey & Lockman 1990). Phoenix does not have the considerable X-ray coverage of M33 and so we did not attempt to derive our own HR criteria, instead we simulated model spectra to confirm that the HR criteria derived by P04 are valid for this work despite the difference in their column densities. Modifications were made where appropriate.

The modified and original P04 criteria used for source classification are summarized in Table 2. Where only one set of criteria are presented, no changes have been made to the original criteria. Where two sets of criteria are presented, the original criteria from P04 are listed underneath the modified criteria in italics. Fig. 3 shows the X-ray hardness ratio plots for all the X-ray sources in Phoenix.

For sources such as foreground stars, galaxies and AGN, it is the additional information at other wavelengths that drives the classification and not the X-ray HRs. Foreground stars are classified based on the ratio of X-ray to optical flux, calculated using their magnitudes given by  $\log(f_X/f_{\text{opt}}) = \log(f_X) + (m_V/2.5) + 5.37$  following Maccacaro et al. (1988). If V-band magnitude information was not available, the average of the  $m_B$  and  $m_R$  values were used in place of  $m_V$ . The distances to all but a handful of stars in our own Galaxy are unknown, making it difficult to assess the level of extinction for an individual foreground star, regardless of the direction we are pointing. As such, no modifications were made to the HR criteria for foreground stars.

The  $HR2 < 0$  criterion for a galaxy classification is a constraint applied when an association was made between a galaxy and one of our X-ray sources. It is primarily to distinguish between a galaxy without an active nucleus and an AGN with a much harder spectrum. There is a smooth transition between the two classifications depending on the relative contributions of star formation and the activity of the central black hole.

The HR criteria are more important for hard sources, SNRs and SSS, where no other information is used in the classification. SSS are generally accepted to be white dwarf systems burning hydrogen on their surface. Any SSS in Phoenix will reside in the bottom left-hand corner of the top panel of the HR plots (see Fig. 3). HRs were calculated for typical SSS (absorbed 30 eV and 50 eV blackbodies) over a range of column densities ( $10^{19}$ – $10^{21} \text{ cm}^{-2}$ ) to see how the difference in the column density to M33 and Phoenix affects the

HR values. All the HRs calculated were well within the original HR limits and so the criteria were left unchanged.

The spectra of SNRs are very similar to those of foreground stars. Following P04, we assumed that all foreground stars have been identified from the correlation with optical data, leaving any remaining sources that fit the HR criteria as SNR candidates. Again, HRs were calculated for typical SNR spectra (absorbed thermal plasma models with temperatures of 0.5 and 1.0 keV) over the same range of column densities as before. All the HRs calculated were within the original criteria and so the criteria were not modified.

The hard classification is arguably the most important for this work. Sources classified as hard are believed to be either unidentified AGN or HMXBs, both of which have absorbed power-law spectra. HRs were calculated for an absorbed power-law spectrum over a range of column densities ( $10^{19}$ – $10^{21} \text{ cm}^{-2}$ ) and photon indices (0.6–3.0). Only the very steepest photon indices ( $\geq 2.8$ ) with low absorption ( $\leq 2 \times 10^{20} \text{ cm}^{-2}$ ) did not fit the hard criterion. Such spectra would imply an AGN with very low intrinsic absorption. The criterion for hard sources was adjusted so that all photon indices with galactic absorption or greater are classified hard.

## 4 SOURCE LIST

The X-ray hardness ratios of all sources in the field of view are displayed in Fig. 3. The red squares are the five sources that are identified in Section 5 for further analysis. The black diamonds are the other 76 sources in the field of view. The hardness ratio criteria are also displayed. Only two X-ray sources have a SIMBAD object within their error circle, five matches were found within the NED data base, 35 matches in the LGGs catalogue and a further three sources in the USNO B1 catalogue. The criteria used for source classification are summarized in Table 2. It is important to note that the source classifications suggested here should be regarded as the proposed nature of the source. The original criteria were derived using the overall properties of large sample populations and not individual sources; consequently, some characteristics of subclasses and sources are not accounted for, such as the X-ray soft, narrow-line Seyfert I galaxies and rare events like stellar flares. A source is ‘*identified*’ if it meets all the criteria for a particular group and is ‘*classified*’ if it meets the majority of the criteria. 19 sources remain unclassified. The source classifications of all the sources in the field of view can be found in Appendix A.

### 4.1 Foreground stars

Foreground stars are expected to lie in the lower left corner of the HR3/HR2 plot (middle panel of Fig. 3). Of the 38 X-ray sources in the field of view with an LGGs or USNO counterpart, one source (14) was positively identified as a star from the SIMBAD data base and another source (56) from the Naval Observatory Merged

**Table 2.** Summary of criteria, identifications and classifications; for more details see text. EHR2 is the error on HR2.

Source type	Selection criteria	Identified	Classified
fg star	$\log\left(\frac{f_X}{f_{\text{opt}}}\right) < -1.0$ and $HR2 < 0.3$ and $HR3 < -0.4$ or not defined	5	1
SNR	$HR1 > 0.1$ and $HR2 < -0.4$ and not an fg star		
AGN	Radio source and classified hard		1
GAL	Optical ID with a galaxy and $HR2 < 0.0$	1	3
SSS	$HR1 < -0.2$ , $HR2\text{-EHR2} < -0.99$ or $HR2$ not defined, $HR3$ and $HR4$ not defined		
hard	$HR2\text{-EHR2} > -0.3$ or only $HR3$ and $HR4$ defined and no other classification		50
	<i><math>HR2\text{-EHR2} &gt; -0.2</math> or only <math>HR3</math> and <math>HR4</math> defined and no other classification</i>		48

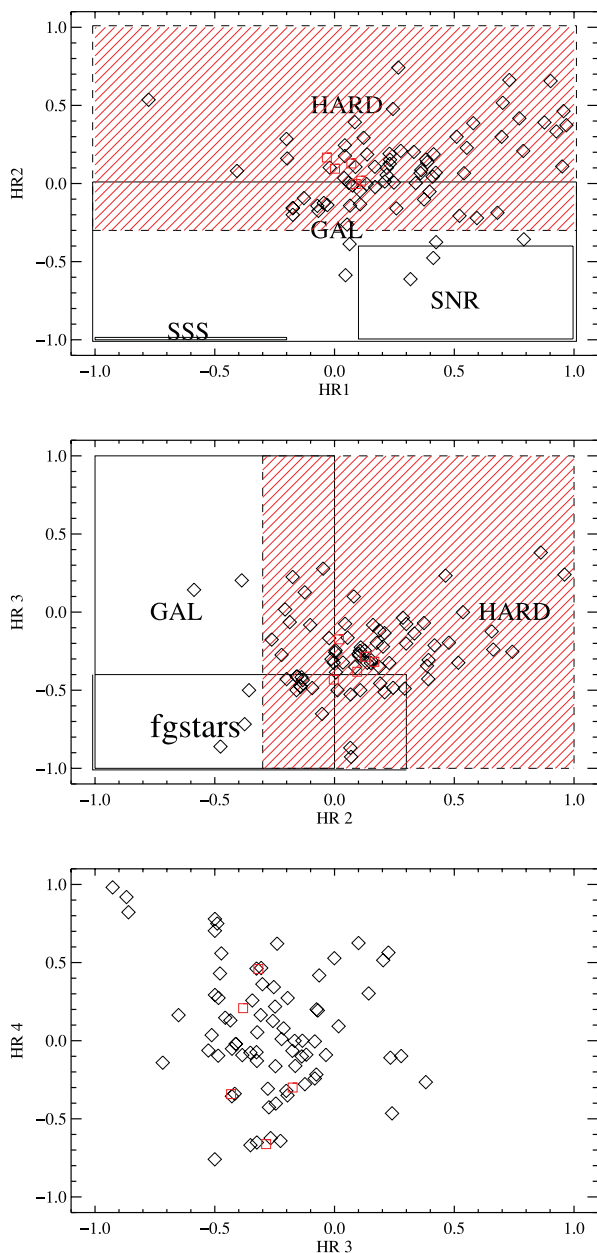


**Figure 3.** X-ray hardness ratios for all sources in the field of view. The regions marked on the plots show the hardness ratio criteria for the different objects. We stress that for objects such as galaxies and foreground stars, it is the information gained at other wavelengths that drives the classification. The errors are not shown for clarity. The red squares are the five sources discussed in Section 5.

Astronomical Dataset (NOMAD) catalogue (Zacharias et al. 2004). A further two sources (27 and 99) were identified as stars based on the optical information available in the LGGs and USNO catalogues.

Sources 78 and 84 all have  $\log(f_x/f_{\text{opt}})$ , indicating a stellar classification, but only source 78 fits the HR criteria within errors, so is also identified as a foreground star. The HR3 value of source 84 is greater than  $-0.4$  required for classification. The optical counterpart is listed in the NOMAD catalogue as being a 14th-magnitude star with colours consistent with being a late K-/early M-type star. The ratio of X-ray to optical flux is also consistent with a K- or

M-type star. We have already stressed in the previous section that for foreground stars, it is the information at other wavelengths that drives the classification. Despite the fact that the HR3 value does not fit the criterion, we feel that the strong agreement of the X-ray to optical flux value and the optical colours warrants a stellar classification. As such source 84 is classified as a foreground star.

#### 4.2 Galaxies and AGN

The X-ray spectrum of a galaxy without an active nucleus is softer than that of a galaxy with an AGN, and so will reside in the lower and left-hand side of the HR1/HR2 and HR2/HR3 plots in Fig. 3. Cross-correlation with the SIMBAD data base identified one source, 39, with a known galaxy in our field of view just outside the H I cloud. This corresponds to SUMSS J015027.5–442537 at  $z = 0.13$ . Four more X-ray sources (10, 31, 43 and 60) have NED objects in their error circles. Sources 10, 31 and 60 all fit the X-ray HR criteria for galaxies. Source 43 is not a galaxy, but listed as an unclassified extragalactic candidate within NED, detected in the radio band. The X-ray source just fits the criteria for a hard source and as such source 43 is classified as an AGN.

#### 4.3 Supersoft sources and supernova remnants

The area of Fig. 3 where the SSS should reside (bottom left-hand corner of the top panel) is remarkably empty. We do not identify or classify any sources as SSS in our field of view. SNRs are expected to fall in the area of the same plot marked SNR. Only two sources fit these HR criteria. They are 14 and 27, two identified foreground stars. As we are confident in our assessment of these sources, we do not find evidence for any SNR in our data.

#### 4.4 Extended sources

Five sources were found to have some measurable extent, these were 36, 41, 81, 91 and 101. With the exception of source 41, these sources are all found on the edge of the field of view and close to a pn chip border. It is more likely that the elongation of the off-axis point spread function (PSF) is not well accounted for at these locations. Source 41 is in very close proximity to 39, the galaxy identified in the SIMBAD data base and discussed in Section 4.2. It has an extent of  $5.7 \pm 0.2$  pixels, which corresponds to  $23.4$  on the sky, greater than the separation of sources 41 and 39 (around  $\sim 19$  arcsec). Along with source 39, source 41 appears to be embedded within a single extended source in the X-ray image. It is likely that these two sources are in fact part of one extended source.

### 5 HMXB CANDIDATES

Of the 81 sources in the field of view, only one source, 48, is coincident with the optical emission of the galaxy. Interestingly, some of the brightest sources in the field of view are offset from the optical emission and spatially coincident with the H I region. 11 sources (34, 35, 48, 52, 54, 56, 58, 61, 62, 66 and 68) lie within the lowest H I contour shown in Fig. 2. The recent bursts of star formation in the western side of the galaxy mean that the location of these sources is compatible with a possible HMXB population. Source 56 is the only identified source in this list. Five sources (34, 35, 52, 61 and 68) have appreciable X-ray emission above 2 keV (with flux values  $> 8 \times 10^{-15}$  erg cm $^{-2}$  s $^{-1}$ ) and occupy an area of  $< 40$  arcmin $^2$ . Their HRs are shown by red squares in Fig. 3. Synthesis models of the cosmic X-ray background by Treister & Urry (2006) and Gilli, Comastri & Hasinger (2007) suggest that we should see  $\sim 2.3^{+1.2}_{-1.9}$

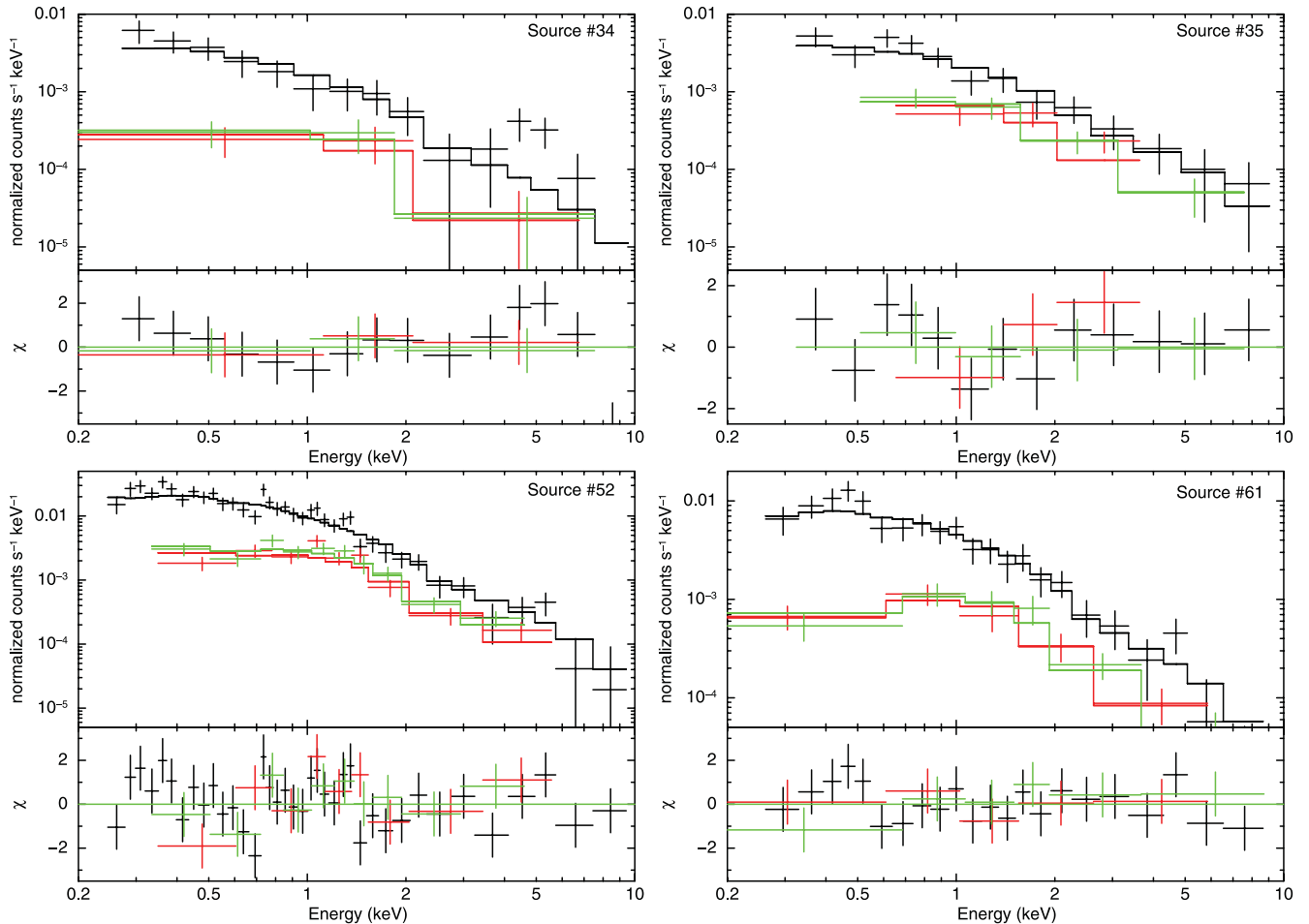


**Figure 4.** X-ray spectra of four of the sources in the H I region and their best-fitting models.

background sources in this energy range and in an area this size. The errors stated are the 90 per cent confidence limits. Whilst five is not an obvious excess over the predicted background numbers, we feel these sources warrant further investigation, particularly as the expected number of HMXBs in Phoenix is small.

Temporal and further spectral analysis is required to distinguish between HMXBs and as yet unidentified AGN. No other X-ray data are available for Phoenix, so we cannot draw comparisons between our results and past observations, but power spectra created from the entire (i.e., no times of high background removed) light curves for all five of these sources showed no evidence for pulsations. 1000 fake pulsar light curves were generated by adding a sinusoid with a period of 100 s to a constant equal to the background-subtracted count rate of the brightest source. The light curves have an amplitude corresponding to a pulsed fraction of 0.3 (the typical value quoted for HMXBs in the SMC; Coe, McBride & Corbet 2010). Random noise was added to every point in the light curve using the IDL program POIDEV, ensuring that the total number of counts in the light curve was conserved. The simulated light curves were then binned with the same bin time as the real light curves. When Lomb–Scargle analysis was performed, only 46 of the 1000 light curves resulted in a significant detection (a  $5\sigma$  detection according to the formula of Horne & Baliunas 1986). An unrealistically high pulsed fraction of 0.6 is required to consistently produce a significant result at 100 s with our total number of counts. Thus, we can conclude that we do

not have the sensitivity to detect pulsations from a typical pulsar in Phoenix using this method.

EPIC spectra were extracted between 200 eV and 10 keV for these sources and were fitted with an absorbed power-law (phabs\*vphabs\*powerlaw) model. The phabs component is fixed at  $1.5 \times 10^{20} \text{ cm}^{-2}$  (Dickey & Lockman 1990) for galactic foreground absorption with elemental abundances from Wilms, Allen & McCray (2000). The vphabs component accounts for absorption in Phoenix and is a free parameter with metal abundances reduced to 0.075, calculated from values given in H09. Throughout the investigation, XSPEC version 12.6.0 was used. The Spectra are shown in Fig. 4, Table 3 contains the best-fitting parameters with 90 per cent confidence errors.

McBride et al. (2008) note that the spectral distribution of Be/X-ray binaries in the SMC is consistent with that of the Milky Way, despite the very different environment. Thus, it seems reasonable to assume that any Be/X-ray binary in Phoenix will fall in the same range of spectral classes (O9V-B2V). Taking the  $M_V$  magnitudes from the stellar flux library of Pickles (1998) and scaling them with the distance to Phoenix predicts V-band magnitudes in the range 18.7–21.2. These values include an  $A_V$  extinction value of 0.062 mag (H09). The distance modulus to Phoenix, 23.1, has an error of  $\pm 0.1$  (H09), which leads to the same error on the magnitudes as calculated for Be/X-ray binaries in Phoenix. Similarly, if we assume that any supergiant X-ray binary present will also fall into

**Table 3.** Properties of the sources detected in the H 1 region. Fluxes are from the model fits in the 0.2–10 keV energy range. For source 68, this information is not available and so the 0.2–12.0 keV flux from the source detection is reported. The ratio of X-ray to optical value has been calculated following the method of Maccacaro et al. (1988) using the flux values from the model fit where possible.

ID	RA (J2000)	Dec. (J2000)	err <sub>1σ</sub> (arcsec)	HR1	HR2	HR3	HR4
35	01:50:41.0	−44:24:32.9	1.5	0.11 ± 0.06	0.02 ± 0.06	−0.17 ± 0.06	−0.30 ± 0.09
68	01:50:45.2	−44:30:34.7	1.6	0.0 ± 0.1	0.17 ± 0.09	−0.3 ± 0.1	0.46 ± 0.09
52	01:50:47.2	−44:27:44.2	1.5	0.09 ± 0.03	0.00 ± 0.03	−0.43 ± 0.03	−0.34 ± 0.06
61	01:50:51.8	−44:29:38.4	1.5	0.07 ± 0.05	0.13 ± 0.04	−0.29 ± 0.05	−0.7 ± 0.1
34	01:51:00.5	−44:24:29.7	1.6	0.00 ± 0.09	0.09 ± 0.08	−0.4 ± 0.1	0.2 ± 0.2
	N <sub>H</sub> 10 <sup>20</sup> cm <sup>−2</sup>	Γ	Flux (erg cm <sup>−2</sup> s <sup>−1</sup> )	χ <sup>2</sup> <sub>r</sub>	m <sub>V</sub>	B − V	log( $\frac{f_X}{f_{opt}}$ )
35	0 <sup>+82</sup>	1.6 <sup>+0.3</sup> <sub>−0.2</sub>	1.9 × 10 <sup>−14</sup>	0.84/15	19.93 ± 0.01	0.44 ± 0.01	−0.38
68			6.3 ± 0.7 × 10 <sup>−14</sup>		21.22 ± 0.02	0.28 ± 0.02	−0.12
52	5.2 <sup>+5.2</sup> <sub>−3.7</sub>	2.1 ± 0.1	6.5 × 10 <sup>−14</sup>	1.21/54	19.49 ± 0.01	0.21 ± 0.01	−0.14
61	5.2 <sup>+12.6</sup> <sub>−5.2</sub>	1.8 ± 0.2	3.8 × 10 <sup>−14</sup>	0.63/28	21.63 ± 0.02	0.51 ± 0.04	0.42
34	0 <sup>+13</sup>	1.9 <sup>+0.4</sup> <sub>−0.3</sub>	1.2 × 10 <sup>−14</sup>	1.58/16	21.47 ± 0.02	0.23 ± 0.04	−0.12

the same range of spectral classes as those already discovered in our own Galaxy and beyond (O8.5I–B3I; Liu et al. 2006) and scale to the distance of Phoenix, we predict *V*-band magnitudes in the range 16.1–16.7 ± 0.1. When searching for HMXB candidates in the SMC, Shtykovskiy & Gilfanov (2005) required that the optical colours of the companion star were  $B - V < 0.20$ . We adopt the same criteria for this work, but take into account the different levels of extinction between the SMC and Phoenix (Rieke & Lebofsky 1985). This leads to the constraint that  $B - V < 0.14$  for any optical counterparts.

Black hole X-ray binaries can exist in several states, the high/soft state, the low/hard state and the quiescent state (which can be considered to be a special case of the low/hard state; Kong et al. 2002). The mass of Phoenix is too low for an LMXB population, but no such restriction applies to the high-mass black hole systems. Our observations are not deep enough to see any quiescent black hole binaries in Phoenix, which would have a flux of about  $\sim 5 \times 10^{-17}$  erg cm<sup>−2</sup> s<sup>−1</sup> (McClintock & Remillard 2006). The luminosity of the high/soft state is typically seen around 10 per cent of the Eddington luminosity (Nowak 1995); for a 6-M<sub>⊙</sub> black hole at the distance of Phoenix, this is  $\sim 8 \times 10^{37}$  erg s<sup>−1</sup> corresponding to a flux of  $\sim 4 \times 10^{-12}$  erg cm<sup>−2</sup> s<sup>−1</sup>. This is an order of magnitude brighter than even the brightest source in our field of view. Consequently, any black hole binaries present in our data set must be in the low/hard state, which is characterized by a power-law spectrum with a photon index of  $\sim 1.7$  and a luminosity of around  $\sim 2$  per cent Eddington or less (Maccacaro 2003; McClintock & Remillard 2006). In the X-ray band, Be/X-ray binaries typically have photon indices of  $\leq 1.4$  (Haberl, Eger & Pietsch 2008b).

### 5.1 Source 34

Source 34 is one of the two spectra with lower signal and as such the parameters for the model fit are not well constrained. The photon index of  $1.9^{+0.4}_{-0.3}$  rules out the possibility that source 34 is a Be/X-ray binary but is consistent with a black hole X-ray binary in Phoenix. The large uncertainty in the parameters and the relatively poor fit mean that this should be treated with caution. The optical counterpart is too faint and red for an early-type star ( $m_V = 21.5$ ,  $B - V = 0.23$ ). Source 34 is most likely an AGN.

### 5.2 Source 35

The X-ray spectrum of source 35 suffers from the same low signal problems as 34. The photon index ( $1.6^{+0.3}_{-0.2}$ ) is just consistent with that of a neutron star in a Be/X-ray binary but comfortably within the range of indices seen for black hole binaries and AGN. The optical counterpart has  $m_V$  consistent with a B-type star in Phoenix, but is well outside the acceptable colour range. As with source 34, source 35 is probably an AGN.

### 5.3 Source 52

The photon index of 52 ( $2.1 \pm 0.1$ ) is too soft for even a black hole X-ray binary, and so source 52 is almost certainly an AGN. The optical information for this source supports this, as again, it is far too red for an early type star in Phoenix ( $B - V = 0.21 \pm 0.01$ ).

### 5.4 Source 61

Source 61 has the greatest X-ray to optical luminosity ratio of our sample and the second greatest in the entire field of view [source 28 has a slightly greater  $\log(f_X/f_{opt})$  value, but is located further from the optical centre of Phoenix and on the eastern side of the galaxy]. The photon index ( $1.8 \pm 0.2$ ) is consistent with a black hole X-ray binary in Phoenix (though also consistent with an AGN). Its optical counterpart is too faint and red for an early-type star ( $m_V = 21.6$ ,  $B - V = 0.51$ ). Source 61 is again probably an AGN.

### 5.5 Source 68

Source 68 is an unfortunately placed X-ray source, falling on a bad column on the EPIC-pn detector and near a chip border in both MOS detectors. The total number of counts for this source was not sufficient to extract a spectrum and so few conclusions can be drawn. The optical counterpart has brightness, but not colours, consistent with an HMXB in Phoenix ( $m_V = 21.2$ ,  $B - V = 0.28$ ) and the 0.2–12.0 keV flux value derived from the source detection ( $6.3 \times 10^{-14}$  erg cm<sup>−2</sup> s<sup>−1</sup>) suggests a luminosity of  $1 \times 10^{36}$  erg s<sup>−1</sup> (assuming source 68 is associated with Phoenix). However, this flux value should be interpreted with care as detector edge effects

may introduce an additional uncertainty that cannot be accounted for. Source 68 is also probably an AGN.

## 6 OTHER SOURCES ASSOCIATED WITH PHOENIX

Interestingly, only one source in our field, 48, is coincident with the most obvious optical emission of the Phoenix dwarf galaxy. Massive black holes have been discovered in nearby dwarf galaxies (for example, see van Wassenhove et al. 2010) and the location of the source, close to what appears to be the centre of the galaxy, led us to consider the source as a possible massive black hole candidate. Although radial velocities have been measured for a handful of stars in Phoenix (Gallart et al. 2001; Irwin & Tolstoy 2002), no information on the location of the dynamical centre is available.

An estimate of the position of the galaxy centre has been obtained by maximizing the number of LGGs sources within a circular region when the centre and size of the region is varied, following the method of Dieball et al. (2010). The uncertainties are estimated via a bootstrapping method. 1000 artificial catalogues were created by sampling with replacement from the original LGGs catalogue. The centre was then estimated for each of these artificial catalogues using the same method as detailed above. The error on our position is taken to be the standard deviation of these centre estimates. Our final result was obtained using a circular region with a 150-pixel (40.5 arcsec) radius, but experiments with other region sizes produced consistent results. The galaxy centre was put at RA =  $01^{\text{h}}51^{\text{m}}8.2 \pm 6.1$  and Dec. =  $-44^{\circ}26'55.9 \pm 7.6$ . This position should be treated with caution as the LGGs catalogue is by no means complete.

Source 48 is situated 40 arcsec away from our centre position with a position error of 1.7 arcsec. This mismatch in positions suggests that source 48 is unlikely to be a massive black hole located at the centre of the Phoenix galaxy. The source hardness ratios are also not consistent with a black hole/AGN in Phoenix. However, the errors on all these values are large and better X-ray and optical data are needed before drawing any firm conclusions about this source.

## 7 DISCUSSION

Of the 81 X-ray sources detected in the *XMM-Newton* field of view, we have categorized six of the sources as foreground stars, four as background galaxies and one as a possible AGN. The majority of the remaining sources in the field of view with optical counterparts have  $\log(f_{\text{X}}/f_{\text{opt}})$  values between  $-1$  and  $1$ , typical of local AGN and high star-forming galaxies (Hornschemeier et al. 2001). Source 96 has the greatest  $\log(f_{\text{X}}/f_{\text{opt}})$  value at  $1.13$ , putting it at the very X-ray brightest end of these objects and a possible BL Lac candidate. Further analysis of five potential HMXB candidates in the field of view suggests that they are all AGN.

We find no evidence for any black hole binaries in Phoenix. The mass of Phoenix is too low for us to expect any LMXBs, so any black hole binaries present would be expected to be high-mass black hole X-ray binaries, in the low/hard state. Belczynski & Ziolkowski (2009) use binary population synthesis models to show that the expected ratio of Be/X-ray binaries with neutron stars to black holes in the Galaxy is relatively high ( $\sim 30$ ). Thus far, not a single Be/X-ray binary has been found to host a black hole. This leaves only black hole supergiant systems. These systems are a small fraction of the total HMXB population in our own Galaxy and are not found at all in the SMC (e.g. Coe et al. 2009). If the

population of HMXBs is as small as predicted, the presence of a black hole supergiant HMXB in Phoenix seems unlikely.

If these sources are spectroscopically confirmed to be AGN, their position behind the gas cloud and their magnitude will make them an excellent tool to further probe the metallicity of this region using the Na I D and Ca II K lines (for e.g. see van Loon et al. 2009). Accurate measurements of the Na and Ca column densities across these sources could tell us more about the gas cloud and may even reveal inhomogeneities in the chemical composition across the region.

Antoniou et al. (2010) report that Be/X-ray binaries in the SMC are found in regions where a burst of star formation occurred  $\sim 25$ – $60$  Myr ago. As such, the five X-ray sources identified offset to the west main stellar body where a strong episode of star formation took place around  $\sim 40$  Myr ago were good candidates for Be/X-ray binaries. However, none of these sources displays all the X-ray and optical characteristics of a Be/X-ray binary. The strongest evidence for a neutron star is periodic modulation of the X-ray flux. We do not have the required sensitivity to detect this in the data but this condition is sufficient, not necessary, for proof of a neutron star's existence.

In general, Be/X-ray binaries are by far the most numerous subclass of HMXBs (Liu et al. 2006) and so have the greatest likelihood of existence in Phoenix. However, as supergiant systems hosting neutron stars are persistent sources of X-rays, we may have a better chance of seeing them in a single epoch. The lack of evidence for any supergiant binaries, with either a black hole or a neutron star secondary, would strongly suggest that they do not exist in Phoenix. This is in line with current predictions based on SFR (Grimm et al. 2003) and is further evidence in support of this relation. Unlike supergiant systems, Be/X-ray binaries are transient in nature and so there is a possibility that a greater population exists than is hinted at here. From our regular observations of the SMC over a 10-year interval, we find that Be/X-ray binaries are in outburst for around  $\sim 10$  per cent of an orbital period and are active, on average, for  $\sim 20$  per cent of the time (Galache et al. 2008; McGowan et al. 2008). It follows that the probability of seeing a particular Be/X-ray binary active at any one moment is about  $\sim 2$  per cent. Should the number of Be/X-ray binaries in Phoenix be limited to just 1–2 systems, then the probability of seeing just one system active at any moment in time is  $< 10$  per cent. Further observations of the Phoenix dwarf galaxy could yet reveal an HMXB population.

This null result is consistent with extending the Log $N$ –Log $S$  relationship reported by Grimm et al. (2003) for HMXBs down to lower luminosities and lower SFRs. Though a positive number would have provided more substantial agreement, it is now evident that a large population of low-luminosity sources does not exist – at least not in Phoenix.

## ACKNOWLEDGMENTS

Based on observations obtained with *XMM-Newton*, an ESA science mission with instruments and contributions directly funded by ESA Member States and NASA. This research has made use of the SIMBAD data base, operated at CDS, Strasbourg, France, and the NASA/IPAC Extragalactic Database (NED), which is operated by the Jet Propulsion Laboratory, California Institute of Technology, under contract with the National Aeronautics and Space Administration. ESB acknowledges support from a Science and Technology Facilities Council studentship.

## REFERENCES

- Antoniou V., Zezas A., Hatzidimitriou D., Kalogera V., 2010, *ApJ*, 716, L140
- Belczynski K., Ziolkowski J., 2009, *ApJ*, 707, 870
- Canterna R., Flower P. J., 1977, *ApJ*, 212, L57
- Coe M. J., Edge W. R. T., Galache J. L., McBride V. A., 2005, *MNRAS*, 356, 502
- Coe M. J. et al., 2009, *IAU Symp.*, 256, 367
- Coe M. J., McBride V. A., Corbet R. H. D., 2010, *MNRAS*, 401, 252
- Dickey J. M., Lockman F. J., 1990, *ARA&A*, 28, 215
- Dieball A., Long K. S., Knigge C., Thomson G. S., Zurek D. R., 2010, *ApJ*, 710, 332
- Dray L. M., 2006, *MNRAS*, 370, 2079
- Galache J. L., Corbet R. H. D., Coe M. J., Laycock S., Schurch M. P. E., Markwardt C., Marshall F. E., Lochner J., 2008, *ApJS*, 177, 189
- Gallart C., Martínez-Delgado D., Gómez-Flechoso M. A., Mateo M., 2001, *AJ*, 121, 2572
- Gilfanov M., 2004, *MNRAS*, 349, 146
- Gilli R., Comastri A., Hasinger G., 2007, *A&A*, 463, 79
- Grimm H.-J., Gilfanov M., Sunyaev R., 2003, *MNRAS*, 339, 793 (G03)
- Haberl F., Eger P., Pietsch W., Corbet R. H. D., Sasaki M., 2008a, *A&A*, 485, 177
- Haberl F., Eger P., Pietsch W., 2008b, *A&A*, 489, 327
- Harris J., Zaritsky D., 2004, *AJ*, 127, 1531
- Harris J., Zaritsky D., 2009, *AJ*, 138, 1243
- Hénault-Brunet V. et al., 2011, *MNRAS*, L372
- Hidalgo S. L., Aparicio A., Martínez-Delgado D., Gallart C., 2009, *ApJ*, 705, 704 (H09)
- Holtzman J. A., Smith G. H., Grillmair C., 2000, *AJ*, 120, 3060
- Hong J., Schlegel E. M., Grindlay J. E., 2004, *ApJ*, 614, 508
- Horne J. H., Baliunas S. L., 1986, *ApJ*, 302, 757
- Hornschemeier A. E. et al., 2001, *ApJ*, 554, 742
- Irwin M., Tolstoy E., 2002, *MNRAS*, 336, 643
- Kong A. K. H., McClintock J. E., Garcia M. R., Murray S. S., Barret D., 2002, *ApJ*, 570, 277
- Liu Q. Z., van Paradijs J., van den Heuvel E. P. J., 2005, *A&A*, 442, 1135
- Liu Q. Z., van Paradijs J., van den Heuvel E. P. J., 2006, *A&A*, 455, 1165
- Lucy L. B., Solomon P. M., 1970, *ApJ*, 159, 879
- McBride V. A., Coe M. J., Negueruela I., Schurch M. P. E., McGowan K. E., 2008, *MNRAS*, 388, 1198
- Maccacaro T., Gioia I. M., Wolter A., Zamorani G., Stocke J. T., 1988, *ApJ*, 326, 680
- Maccarone T. J., 2003, *A&A*, 409, 697
- McClintock J. E., Remillard R. A., 2006, *Compact Stellar X-ray Sources*. Cambridge Univ. Press, Cambridge, p. 157
- McGowan K. E. et al., 2008, *MNRAS*, 383, 330
- Martínez-Delgado D., Gallart C., Aparicio A., 1999, *AJ*, 118, 862
- Massey P., Olsen K. A. G., Hodge P. W., Jacoby G. H., McNeill R. T., Smith R. C., Strong S. B., 2007, *AJ*, 133, 2393
- Mateo M. L., 1998, *ARA&A*, 36, 435
- Menzies J., Feast M., Whitelock P., Olivier E., Matsunaga N., da Costa G., 2008, *MNRAS*, 385, 1045
- Monet D. G. et al., 2003, *AJ*, 125, 984
- Nowak M. A., 1995, *PASP*, 107, 1207
- Pickles A. J., 1998, *PASP*, 110, 863
- Pietsch W., Misanovic Z., Haberl F., Hatzidimitriou D., Ehle M., Trinchieri G., 2004, *A&A*, 426, 11 (P04)
- Rieke G. H., Lebofsky M. J., 1985, *ApJ*, 288, 618
- Russell S. C., Dopita M. A., 1992, *ApJ*, 384, 508
- Schuster H.-E., West R. M., 1976, *A&AR*, 49, 129
- Shtykovskiy P., Gilfanov M., 2005, *MNRAS*, 362, 879
- Stella L., White N. E., Rosner R., 1986, *ApJ*, 308, 669
- Strüder L. et al., 2001, *A&A*, 365, L18
- Treister E., Urry C. M., 2006, *ApJ*, 652, L79
- Turner M. J. L. et al., 2001, *A&A*, 365, L27
- van de Rydt F., Demers S., Kunkel W. E., 1991, *AJ*, 102, 130
- van Loon J. T., Smith K. T., McDonald I., Sarre P. J., Fossey S. J., Sharp R. G., 2009, *MNRAS*, 399, 195
- van Wassenhove S., Volonteri M., Walker M. G., Gair J. R., 2010, *MNRAS*, 408, 1139
- Watson M. G. et al., 2009, *A&A*, 493, 339
- Wilms J., Allen A., McCray R., 2000, *ApJ*, 542, 914
- Yokogawa J., Imanishi K., Tsujimoto M., Nishiuchi M., Koyama K., Nagase F., Corbet R. H. D., 2000, *ApJS*, 128, 491
- Young L. M., Lo K. Y., 1997, *ApJ*, 490, 710
- Young L. M., Skillman E. D., Weisz D. R., Dolphin A. E., 2007, *ApJ*, 659, 331
- Zacharias N., Monet D. G., Levine S. E., Urban S. E., Gaume R., Wycoff G. L., 2004, *AAS*, 36, 1418

## APPENDIX A: COMPLETE X-RAY SOURCE LIST

**Table A1.** Properties of all the sources in the *XMM-Newton* field of view. Count rates and fluxes are both given for the 0.2–12 keV energy range. Here,  $\log(f_x/f_{\text{opt}})$  is calculated from the 0.2–4.5 keV flux values and the optical data available in the LGGs or USNO catalogue. The classification column follows the designation in the text with *classified* sources in square brackets. Unclassified sources are listed as ‘unclass’.

ID	RA (J2000)	Dec. (J2000)	err <sub>1σ</sub> (arcsec)	Count rate (10 <sup>-3</sup> s <sup>-1</sup> )	Flux (10 <sup>-14</sup> erg cm <sup>-2</sup> s <sup>-1</sup> )	$\log\left(\frac{f_x}{f_{\text{opt}}}\right)$	HR1	HR2	HR3	HR4	Classification
47	01:49:43.7	-44:26:46.4	2.1	10 ± 1	2.4 ± 0.8	-0.05	0.0 ± 0.1	-0.1 ± 0.1	0.1 ± 0.2	-1.0 ± 0.3	[hard]
23	01:49:54.1	-44:22:49.3	1.7	12 ± 2	8 ± 1		0.7 ± 0.3	0.7 ± 0.1	-0.2 ± 0.1	0.6 ± 0.1	[hard]
36	01:49:54.4	-44:25:04.0	1.7	11 ± 1	8 ± 1		0.4 ± 0.2	0.1 ± 0.1	-0.9 ± 0.2	0.98 ± 0.07	unclass
81	01:49:54.8	-44:32:27.9	1.6	24 ± 2	12 ± 2		-0.1 ± 0.1	0.1 ± 0.1	0.1 ± 0.1	0.62 ± 0.06	[hard]
91	01:50:02.1	-44:34:56.2	1.8	17 ± 2	6 ± 2		-0.78 ± 0.09	0.5 ± 0.1	0.0 ± 0.1	0.53 ± 0.07	[hard]
15	01:50:03.5	-44:21:23.5	1.7	5.9 ± 0.8	0.6 ± 0.3		0.2 ± 0.1	0.1 ± 0.1	-0.5 ± 0.2	0.8 ± 0.3	unclass
84	01:50:06.8	-44:33:20.0	1.8	11 ± 1	1.0 ± 0.9	-3.10	0.05 ± 0.09	-0.6 ± 0.1	0.1 ± 0.3	0.3 ± 0.3	[fgstar]
25	01:50:07.6	-44:22:54.4	1.6	24 ± 1	3.9 ± 0.7	-0.02	0.04 ± 0.06	0.04 ± 0.06	-0.32 ± 0.08	0.1 ± 0.1	[hard]
31	01:50:11.5	-44:23:23.2	1.5	30 ± 1	5.3 ± 0.7	0.18	0.11 ± 0.05	-0.13 ± 0.05	-0.43 ± 0.07	0.1 ± 0.1	[gal]
49	01:50:12.7	-44:26:58.6	1.5	33 ± 1	11 ± 1	-0.30	0.70 ± 0.07	0.52 ± 0.04	-0.32 ± 0.04	-0.13 ± 0.0	[hard]
33	01:50:14.9	-44:24:04.2	1.6	7.0 ± 0.8	1.4 ± 0.4		0.9 ± 0.2	0.66 ± 0.09	-0.1 ± 0.1	-0.3 ± 0.2	[hard]
70	01:50:15.0	-44:30:41.1	1.6	8 ± 1	2.2 ± 0.7		0.1 ± 0.1	-0.1 ± 0.2	-0.5 ± 0.1	0.4 ± 0.2	unclass
96	01:50:15.4	-44:35:51.4	1.5	67 ± 2	19 ± 2	1.13	0.23 ± 0.04	0.15 ± 0.04	-0.33 ± 0.04	-0.07 ± 0.08	[hard]
7	01:50:19.4	-44:39:56.0	1.5	58 ± 2	13 ± 2	-0.44	-0.17 ± 0.04	-0.20 ± 0.05	-0.43 ± 0.07	-0.4 ± 0.3	unclass
71	01:50:19.7	-44:30:47.7	1.6	19 ± 1	3.4 ± 0.5	0.87	0.04 ± 0.08	0.18 ± 0.07	-0.20 ± 0.07	-0.4 ± 0.1	[hard]
3	01:50:20.5	-44:17:10.6	1.7	11 ± 1	6 ± 1		0.1 ± 0.2	0.4 ± 0.1	-0.3 ± 0.1	0.5 ± 0.1	[hard]
42	01:50:20.7	-44:25:55.5	1.7	6.9 ± 0.8	3.0 ± 0.7	0.08	0.2 ± 0.1	0.0 ± 0.1	-0.5 ± 0.2	0.7 ± 0.1	unclass
4	01:50:23.8	-44:17:08.7	1.6	17 ± 2	2.2 ± 0.6	0.15	0.1 ± 0.1	0.0 ± 0.1	-0.3 ± 0.1	0.4 ± 0.1	[hard]
14	01:50:24.2	-44:20:49.1	1.6	6.8 ± 0.7	0.9 ± 0.4	-4.55	0.32 ± 0.08	-0.61 ± 0.09	-1.0 ± 0.4	1.0 ± 1.9	fgstar
39	01:50:28.1	-44:25:35.2	1.7	11.6 ± 0.7	1.5 ± 0.3	-0.90	0.79 ± 0.05	-0.36 ± 0.06	-0.5 ± 0.1	-0.8 ± 0.3	gal
11	01:50:28.7	-44:19:27.7	1.7	8.6 ± 0.8	5.8 ± 0.9		0.3 ± 0.3	0.7 ± 0.1	-0.3 ± 0.1	0.2 ± 0.1	[hard]
41	01:50:29.0	-44:25:51.7	1.6	15.3 ± 0.8	3.0 ± 0.4		0.40 ± 0.06	-0.05 ± 0.06	-0.65 ± 0.07	0.3 ± 0.1	[gal]
82	01:50:32.9	-44:32:32.2	1.6	9.4 ± 0.8	1.4 ± 0.4	0.27	0.2 ± 0.1	0.10 ± 0.09	-0.3 ± 0.1	-0.6 ± 0.3	[hard]
90	01:50:38.5	-44:34:45.5	1.5	60 ± 2	9.2 ± 0.8	0.27	-0.03 ± 0.03	-0.14 ± 0.04	-0.42 ± 0.05	-0.3 ± 0.1	unclass
1	01:50:39.2	-44:40:25.5	1.9	9 ± 2	5 ± 2		-0.2 ± 0.2	0.3 ± 0.2	0.0 ± 0.2	-0.1 ± 0.4	[hard]
56	01:50:42.7	-44:29:04.5	1.5	22.4 ± 0.8	2.5 ± 0.2	-2.20	0.42 ± 0.04	-0.38 ± 0.04	-0.72 ± 0.06	-0.1 ± 0.2	fgstar
99	01:50:43.6	-44:36:13.1	1.6	12 ± 1	2.6 ± 0.8	-4.46	0.2 ± 0.1	0.19 ± 0.09	-0.5 ± 0.1	0.1 ± 0.2	fgstar
54	01:50:45.3	-44:28:29.2	1.6	7.1 ± 0.5	1.5 ± 0.3	0.08	0.26 ± 0.09	-0.16 ± 0.09	-0.5 ± 0.1	0.3 ± 0.2	unclass
12	01:50:46.6	-44:20:31.6	1.7	4.4 ± 0.5	2.0 ± 0.5		0.4 ± 0.2	0.0 ± 0.1	-0.1 ± 0.2	0.2 ± 0.2	[hard]
100	01:50:54.5	-44:36:23.7	1.7	9.4 ± 0.9	2.3 ± 0.6	-0.31	-0.1 ± 0.1	-0.1 ± 0.1	-0.5 ± 0.2	0.6 ± 0.2	unclass
62	01:50:54.6	-44:29:44.7	1.7	3.4 ± 0.4	0.9 ± 0.3	-0.07	0.1 ± 0.2	0.0 ± 0.2	0.3 ± 0.2	-0.1 ± 0.2	[hard]
66	01:51:00.1	-44:30:19.6	1.7	13 ± 1	1.4 ± 0.3		0.4 ± 0.1	0.2 ± 0.1	-0.3 ± 0.1	0.2 ± 0.1	[hard]
9	01:51:02.9	-44:18:52.4	1.5	21 ± 1	9.4 ± 0.8		0.77 ± 0.09	0.42 ± 0.06	-0.21 ± 0.06	0.08 ± 0.07	[hard]
16	01:51:03.2	-44:21:39.3	1.8	3.5 ± 0.4	1.0 ± 0.3		0.3 ± 0.2	0.2 ± 0.1	-0.2 ± 0.1	0.0 ± 0.2	[hard]
58	01:51:04.3	-44:29:23.7	1.6	9.9 ± 0.6	1.5 ± 0.2	0.07	0.05 ± 0.06	-0.26 ± 0.07	-0.2 ± 0.1	-0.1 ± 0.1	unclass
48	01:51:04.6	-44:26:49.2	1.7	2.8 ± 0.3	0.4 ± 0.2	-0.61	-0.2 ± 0.1	-0.2 ± 0.2	-0.4 ± 0.2	0.0 ± 0.4	unclass
10	01:51:09.0	-44:18:56.0	1.6	20.7 ± 0.8	4.3 ± 0.5	0.21	-0.13 ± 0.04	-0.09 ± 0.05	-0.49 ± 0.07	-0.1 ± 0.2	[gal]
21	01:51:13.7	-44:22:46.2	1.7	8.7 ± 0.9	1.1 ± 0.3		0.9 ± 0.1	0.3 ± 0.1	-0.1 ± 0.1	-0.1 ± 0.1	[hard]
28	01:51:13.8	-44:23:07.8	1.6	19 ± 1	3.2 ± 0.4	0.47	0.22 ± 0.08	0.05 ± 0.08	-0.16 ± 0.08	-0.2 ± 0.1	[hard]
38	01:51:14.9	-44:25:09.9	1.6	9.8 ± 0.5	1.5 ± 0.2		0.39 ± 0.07	0.14 ± 0.06	-0.32 ± 0.07	-0.7 ± 0.1	[hard]
2	01:51:17.6	-44:40:14.9	1.6	9 ± 1	2.3 ± 0.8		0.1 ± 0.1	-0.4 ± 0.1	0.2 ± 0.2	0.5 ± 0.3	unclass

Table A1 – continued

ID	RA (J2000)	Dec. (J2000)	err <sub>σ</sub> (arcsec)	Count rate (10 <sup>-3</sup> s <sup>-1</sup> )	Flux (10 <sup>-14</sup> erg cm <sup>-2</sup> s <sup>-1</sup> )	$\log \left( \frac{f_x}{f_{\text{opt}}} \right)$	HR1	HR2	HR3	HR4	Classification
22	01:51:21.6	-44:22:43.2	1.6	16 ± 1	1.3 ± 0.2		0.04 ± 0.09	0.24 ± 0.08	-0.48 ± 0.08	0.27 ± 0.08	unclass
55	01:51:22.5	-44:28:39.6	1.6	7.3 ± 0.5	1.1 ± 0.2		0.14 ± 0.09	0.19 ± 0.08	-0.35 ± 0.09	-0.7 ± 0.2	[hard]
13	01:51:23.3	-44:20:44.0	1.6	7.1 ± 0.6	1.7 ± 0.3		0.9 ± 0.1	0.39 ± 0.07	-0.43 ± 0.08	-0.1 ± 0.2	[hard]
92	01:51:24.7	-44:35:09.2	1.6	21 ± 1	10.0 ± 0.9	-0.82	1.0 ± 0.6	0.86 ± 0.07	0.38 ± 0.05	-0.27 ± 0.0	[hard]
50	01:51:24.9	-44:27:23.9	1.6	6.8 ± 0.6	1.6 ± 0.3		0.2 ± 0.1	0.0 ± 0.1	-0.2 ± 0.1	0.0 ± 0.2	[hard]
72	01:51:25.9	-44:31:07.4	1.7	10 ± 1	2.4 ± 0.5		-0.1 ± 0.2	-0.2 ± 0.2	0.2 ± 0.2	0.6 ± 0.1	unclass
29	01:51:26.0	-44:23:11.9	1.7	4.8 ± 0.5	1.0 ± 0.2		0.4 ± 0.1	0.1 ± 0.1	-0.5 ± 0.1	-0.1 ± 0.2	unclass
20	01:51:28.6	-44:22:39.1	1.9	2.9 ± 0.4	0.3 ± 0.1	-0.84	1.0 ± 0.2	0.1 ± 0.1	-0.2 ± 0.1	-0.6 ± 0.3	[hard]
73	01:51:30.1	-44:30:54.3	1.5	23.2 ± 0.9	5.2 ± 0.5	0.12	0.25 ± 0.05	0.01 ± 0.05	-0.39 ± 0.06	-0.1 ± 0.1	[hard]
65	01:51:30.2	-44:29:57.0	1.6	17 ± 2	3.0 ± 0.5		0.4 ± 0.1	0.19 ± 0.09	-0.1 ± 0.1	-0.1 ± 0.1	[hard]
27	01:51:30.6	-44:22:54.9	1.6	9.0 ± 0.5	1.2 ± 0.2	-1.41	0.41 ± 0.06	-0.48 ± 0.06	-0.9 ± 0.1	0.8 ± 0.2	fgstar
74	01:51:32.1	-44:31:11.3	1.7	5.4 ± 0.6	1.6 ± 0.4		0.5 ± 0.2	0.1 ± 0.1	-0.9 ± 0.1	0.9 ± 0.1	unclass
59	01:51:37.3	-44:29:27.3	1.6	7.6 ± 0.6	1.4 ± 0.3		0.36 ± 0.09	0.09 ± 0.08	-0.4 ± 0.1	-0.1 ± 0.2	[hard]
63	01:51:39.7	-44:29:46.8	1.6	9.9 ± 0.7	3.3 ± 0.5		0.34 ± 0.09	0.00 ± 0.08	-0.3 ± 0.1	0.1 ± 0.1	[hard]
8	01:51:41.3	-44:18:27.3	1.5	35 ± 1	7.0 ± 0.7	-0.02	0.06 ± 0.04	0.00 ± 0.04	-0.25 ± 0.05	-0.40 ± 0.09	[hard]
6	01:51:41.4	-44:18:13.3	1.7	6.5 ± 0.9	2.6 ± 0.6		0.1 ± 0.2	0.3 ± 0.2	-0.5 ± 0.2	0.7 ± 0.1	unclass
67	01:51:41.8	-44:30:13.6	1.7	7.2 ± 0.6	2.3 ± 0.4		0.5 ± 0.1	-0.2 ± 0.1	0.0 ± 0.1	0.1 ± 0.1	unclass
85	01:51:42.0	-44:33:21.7	1.6	11.9 ± 0.9	2.9 ± 0.7		0.3 ± 0.1	0.21 ± 0.07	-0.51 ± 0.09	0.0 ± 0.2	unclass
45	01:51:42.7	-44:26:07.7	1.6	13.0 ± 0.7	3.1 ± 0.4		0.23 ± 0.07	0.13 ± 0.06	-0.25 ± 0.07	-0.2 ± 0.1	[hard]
17	01:51:43.3	-44:21:55.9	1.9	4.6 ± 0.6	1.8 ± 0.5		1.0 ± 0.1	0.4 ± 0.1	-0.1 ± 0.1	0.2 ± 0.2	[hard]
94	01:51:44.5	-44:35:31.1	1.7	11 ± 1	6 ± 1		0.6 ± 0.1	0.2 ± 0.1	-0.3 ± 0.1	0.5 ± 0.2	[hard]
18	01:51:45.6	-44:22:00.0	1.6	13.1 ± 0.8	2.3 ± 0.4	-0.58	-0.02 ± 0.07	0.10 ± 0.07	-0.28 ± 0.08	-0.3 ± 0.2	[hard]
101	01:51:49.9	-44:37:04.5	1.7	12 ± 1	2.5 ± 0.7	-0.48	-0.2 ± 0.1	0.2 ± 0.1	-0.1 ± 0.1	0.0 ± 0.2	[hard]
78	01:51:51.6	-44:32:17.5	1.8	4.1 ± 0.6	0.6 ± 0.4	-2.37	0.6 ± 0.2	-0.2 ± 0.2	-0.3 ± 0.2	-0.4 ± 0.4	fgstar
43	01:51:52.1	-44:25:46.1	1.6	10.5 ± 0.6	1.3 ± 0.2	0.24	0.13 ± 0.07	0.00 ± 0.07	-0.32 ± 0.09	-1.0 ± 0.2	[AGN]
80	01:51:55.4	-44:32:22.5	1.6	15 ± 1	4.0 ± 0.7		0.79 ± 0.08	0.21 ± 0.08	-0.13 ± 0.08	0.0 ± 0.1	[hard]
60	01:51:56.0	-44:29:28.7	1.6	10 ± 1	3.1 ± 0.7	-0.56	0.7 ± 0.1	-0.2 ± 0.1	-0.1 ± 0.2	0.4 ± 0.1	[gal]
83	01:51:57.2	-44:23:55.3	1.6	16 ± 1	3.9 ± 0.8		0.70 ± 0.09	0.30 ± 0.06	-0.20 ± 0.07	-0.3 ± 0.2	[hard]
30	01:51:57.4	-44:32:06.1	1.6	18 ± 1	5.7 ± 0.7	-0.20	0.09 ± 0.08	0.11 ± 0.07	-0.25 ± 0.08	0.2 ± 0.1	[hard]
57	01:52:00.7	-44:29:14.6	1.6	8.5 ± 0.8	4.0 ± 0.7		1.0 ± 0.2	0.5 ± 0.1	0.23 ± 0.09	-0.1 ± 0.1	[hard]
97	01:52:00.9	-44:35:54.5	1.6	25 ± 1	5.0 ± 0.9		0.37 ± 0.07	-0.10 ± 0.06	-0.08 ± 0.07	-0.2 ± 0.1	[hard]
19	01:52:02.6	-44:22:08.7	1.6	12.1 ± 0.9	3.0 ± 0.6		0.5 ± 0.1	0.30 ± 0.08	-0.08 ± 0.08	-0.2 ± 0.1	[hard]
26	01:52:11.1	-44:22:56.2	1.7	5.0 ± 0.6	5 ± 1		1.0 ± 1.9	0.96 ± 0.07	0.2 ± 0.1	-0.5 ± 0.2	[hard]
5	01:52:11.3	-44:18:08.8	1.6	27 ± 3	31 ± 6		0.6 ± 0.1	0.4 ± 0.1	-0.3 ± 0.1	0.3 ± 0.2	[hard]
37	01:52:25.0	-44:25:16.5	1.7	9.1 ± 0.9	11 ± 2		0.2 ± 0.2	0.5 ± 0.1	-0.2 ± 0.1	0.3 ± 0.1	[hard]

This paper has been typeset from a TeX/L<sup>A</sup>T<sub>E</sub>X file prepared by the author.